

1 **Properties of hail storms over China and the United States**
2 **from the Tropical Rainfall Measuring Mission**

3

4 Authors: Xiang Ni^{1,2}, Chuntao Liu², Qinghong Zhang^{1,*}, and Daniel J. Cecil³

5

6 ¹Department of Atmospheric and Oceanic Sciences, School of Physics, Peking

7 University, Beijing, China,

8 ²Department of Physical and Environmental Sciences, Texas A&M University at

9 Corpus Christi, Texas, USA,

10 ³NASA Marshall Space Flight Center, Huntsville, Alabama, USA,

11

12 *Corresponding author: Qinghong Zhang (qzhang@pku.edu.cn)

13

14 **Key Points:**

15 ● Hail reports in China and U.S. are collocated with TRMM Precipitation Features.

16 ● Hailstorms in U.S. have larger hail diameter and show stronger convective

17 characteristics than those in China.

18 ● Full spectra of hail size vs. radar and passive microwave observations have been

19 constructed.

20

21 **Abstract**

22 A 16-yr record of hail reports over the south U.S. and from weather stations in China
23 are collocated with Precipitation Features (PF) derived from the Tropical Rainfall
24 Measuring Mission (TRMM) radar and passive microwave observations. Differences
25 in the way hail is reported in the two nations make it difficult to draw meaningful
26 conclusions about storm frequency. But taking the two together yields a wide spectrum
27 of hail sizes, suitable for comparing with remote sensing measurements. While U.S.
28 hail reports are dominated by cases with hail size greater than 19 mm, hail reports in
29 China mostly include diameters of 1-10 mm and mostly occur over the Tibetan Plateau.
30 The fraction of PFs collocated with hail reports (hail PFs) reaches 3% in the plains of
31 the U.S. In China, the fraction is higher in high elevation regions than low elevation
32 regions. Hail PFs (as reported in the U.S.) show lower brightness temperatures, higher
33 lightning flash rates, stronger maximum reflectivity, and higher echo tops than those
34 with smaller hail, as reported in China. The average near surface maximum reflectivity
35 of hail PFs at high elevations (≥ 2000 m) in China is about 5 dB smaller than those at
36 low elevations. Larger hail is reported with PFs having stronger maximum reflectivity
37 above 6 km, though the median of maximum reflectivity values at levels below 5 km is
38 similar among the storms with large and small hail sizes.

39

40 **1. Introduction**

41 As a natural disaster, hailstorms are a major threat to agriculture and society and could
42 cause appreciable damage to property. In recent years, regional climatologies of hail
43 events based upon ground-based observations, including surface weather station reports,
44 hailpad reports, radar-based algorithm, and insurance data, have been studied
45 worldwide [*Changnon and Changnon, 2000; Vinet, 2000; Knight and Knight, 2001;*
46 *Zhang et al., 2008; Tuovinen et al., 2009; Cintineo et al., 2012*]. Hailpads in some
47 European countries have been used to study the regional hail intensity and frequency in
48 limited periods of time and regions [*Vinet, 2000; Berthet et al., 2011; Manzato, 2012*].
49 Weather station hail reports in China, North Korea, and U.S. have shown downward
50 trends of hail days in recent decades [*Changnon and Changnon, 2000; Xie et al., 2008;*
51 *Changnon et al., 2009; Kim and Ni, 2015*]. However, the hail reports from stations could
52 be dominated by hail with small diameters [*Xie et al., 2010*] and the hailstorms far from
53 stations could be omitted. The *Storm Data* of the National Climatic Data Center (NCDC)
54 provides details of hail reports over the U.S [*Schaefer et al., 2004*]. These reports could
55 be biased towards high population regions [*Dobur, 2005*]. The standards for reporting
56 hail vary by location and also varies in time. The diversity of the human hail reports
57 collections could lead to inconsistent hail climatology over various regions. This
58 motivates us to seek a uniform observation method to study the characteristics of
59 hailstorms globally.

60

61 Hailstorms are directly related to intense convection with strong updrafts, high radar
62 reflectivity, and often lightning. *Deierling and Petersen* [2008] confirmed the
63 relationship between total lightning and updraft volume above -5 °C. The majority of
64 severe storm reports were associating with lightning [*Carey et al.*, 2003]. During the
65 hail suppression experiments in the 1970s [*Mather et al.*, 1976; *Waldvogel et al.*, 1979],
66 the surface hail occurrences were found related to the height of 45 dBZ at 1.4 km above
67 the freezing level according to single radar observations. This relationship has been
68 employed in the hail algorithm by National Weather Service during 1980s and 1990s
69 [*Heinselman and Ryzhkov*, 2006].

70

71 In intense convective systems, the scattering of microwave radiances by hail or graupel
72 aloft could cause extremely low microwave brightness temperature (TB) seen from
73 satellites. Low 37 GHz Polarization Corrected Temperatures (PCT, *Spencer et al.*
74 [1989]) are found corresponding to high radar reflectivity through a deep layer [*Cecil*,
75 2011]. *Cecil* [2009] described the basis for interpreting maps of storms with low 37
76 GHz brightness temperature as a global pseudo-climatology of large hail. On this basis,
77 global large hail climatologies were generated using different kinds of microwave
78 radiometer sensors [*Cecil and Blankenship*, 2012; *Ferraro et al.*, 2015]. In these studies,
79 relationships between 37 GHz PCT and hail events are built upon the surface hail
80 reports only over the U.S. *Cecil and Blankenship* [2012] compared their satellite-based
81 climatology with a ground-based climatology compiled by *Williams* [1973] and *Frisby*

82 *and Sansom* [1967]. The ground-based climatology shows hail maxima across
83 mountainous areas that are presumably more prone to graupel and small hail than to the
84 larger hail that is the focus of the satellite-based studies. This leads to questions about
85 differences in properties of the reported hail in different regions, and differences in the
86 remote sensing properties of the associated storms. In this study, we draw such
87 comparisons using a hail database from China that is dominated by small hail (< 5 mm)
88 falling over high terrain, and a database from the U.S. featuring larger hail at lower
89 elevations.

90

91 The multiple satellite sensors on the Tropical Rainfall Measuring Mission (TRMM)
92 [*Kummerow et al.*, 1998] satellite, including TRMM Microwave Imager (TMI), the
93 precipitation radar (PR), Visible and Infrared Scanner (VIRS), and Lightning Imaging
94 System (LIS), have been widely used to study storm structure in the tropical and
95 subtropical regions between 36°S~36°N [*Nesbitt and Zipser*, 2000; *Liu and Zipser*,
96 2005; *Zipser et al.*, 2006; *Xu*, 2012; *Hamada et al.*, 2015]. The objective of this paper
97 is to use the 16-yr TRMM observations to compare the properties of hailstorms of
98 various intensities over China and the U.S. The relationships between radar and passive
99 microwave remote sensing observations, such as the radar reflectivity profiles and PCTs,
100 and microphysical properties of hailstorms are summarized and compared over China
101 and the U.S. Given differences in the underlying hail databases, these are essentially
102 comparisons between storms with small hail or graupel (in China) versus those with

103 large hail (in the U.S.). The sources of hail reports and the approach of collocation with
104 TRMM observations are described in section 2. Section 3 discusses hailstorm properties
105 over China and the U.S. and their differences. A summary is given in section 4.

106

107 **2. Data and methodology**

108 **2.1 TRMM precipitation feature**

109 The TRMM Precipitation Feature (PF) database [Liu *et al.*, 2008] is used to study
110 properties of hailstorms in this paper. In the PF database, measurements from multiple
111 instruments on TRMM, including VIRS infrared and TMI TB, LIS lightning flash rates,
112 and PR reflectivity, are collocated using the coordinates of PR pixels as the standard
113 grids. Based on the collocated TRMM dataset, different criteria are used to define the
114 PF as the Level-2 products. Radar Precipitation Features (RPFs) during 1998–2013
115 used in this study are defined by grouping the contiguous pixels (≥ 4 pixels) in a
116 TRMM orbit with nonzero surface rainfall from the TRMM 2A25 algorithm [Iguchi *et*
117 *al.*, 2000, 2009]. The properties of each PF are summarized, including the maximum
118 radar reflectivity profile, minimum 85 and 37 GHz PCTs (MIN85PCT, MIN37PCT),
119 lightning flash rate, and maximum 30 and 40 dBZ echo top temperature (TMAXHT30,
120 TMAXHT40). To derive the temperature at echo tops, the temperature profile is
121 temporally and spatially interpolated to each PF time and location from 6 hourly 0.75
122 degree ERA-Interim reanalysis dataset [Dee *et al.*, 2011]. Because hail events mainly

123 occur in boreal spring and summer over China and U.S., the data during the winter
124 season (December-February) are excluded from all discussion in this paper.

125

126 **2.2 Hail report**

127 The hail reports in China during 1998-2013 are compiled based on two datasets from
128 the China Meteorological Administration (CMA). The first one is the hail dataset
129 according to surface weather station observations, including hail start time and end time.
130 This dataset has been applied in the hail climatology study in the past [*Xie et al.*, 2008;
131 *Zhang et al.*, 2008]. Recently, Maximum Hail Diameters (MHDs) have been extracted
132 from the Surface Weather Report dataset (SWR) and quality controlled by CMA. In the
133 SWR, hail size is recorded as the special weather phenomena following the World
134 Meteorological Organization (WMO) meteorological codes
135 (<http://www.wmo.int/pages/prog/www/WMOCodes.html>). According to WMO codes,
136 ice particle larger than 5 mm is defined as hail, and ice pellets, graupel, and small hail
137 are all recorded in the station observation reports. To understand the transition from
138 graupel to hail, we choose to use all the reports of solid ice precipitation with size
139 greater than or equal to 1 mm in this study. Most MHD records from weather stations
140 in China are smaller than the hail definition (5 mm) of WMO and are referred to as
141 graupel events. In total, 4517 graupel and 2158 hail reports with occurrence time and
142 MHD are found at 319 stations south of 36°N during the study period (1998-2013). As
143 shown in Fig. 1a, most of these stations are over the Tibet plateau, where their mean

144 MHDs are mostly smaller than 5 mm.

145

146 The hail events in U.S. are compiled by National Oceanic and Atmospheric
147 Administration (NOAA) [Schaefer and Edwards, 1999]. Different from the weather
148 station hail reports in China, the U.S. collects severe storm reports from the public [Witt
149 *et al.*, 1998], which increases the number of hail reports for more complete verification
150 [Ortega *et al.*, 2009, 2016]. The hail reports from NOAA contain the hail size, location
151 and time. This hail storm data has been extensively used to study hail climatology and
152 hail storm properties observed from satellites [Jirak *et al.*, 2003; Cecil, 2009; Gallo *et*
153 *al.*, 2012; Allen and Tippett, 2015; Ferraro *et al.*, 2015]. Hail smaller than 1 inch (25
154 mm) does not qualify as verifying a severe thunderstorm warning in the U.S., so records
155 of smaller hail are incomplete. A 0.75 inch (19 mm) threshold was used for severe
156 thunderstorm warnings before 2010. For the hail reports south of 36°N, the minimum
157 hail size reported in the U.S. is 0.25 inch (6.25 mm), which is greater than the WMO
158 hail definition. In total, 62842 of U.S. hail reports are found south of 36°N during the
159 study period. Because of different reporting procedures, distinctions between the
160 databases from China and the U.S. can generally be thought of as distinctions between
161 graupel/small hail and larger hail.

162 **2.3 Define hail PFs**

163 Taking advantage of the detailed time and location of hail reports in China and U.S., it
164 is possible to collocate hail reports with the nearest TRMM observations. The PFs

165 possibly associated with hail are searched within 1° and one hour from the PF's centroid
166 location and observation time. If multiple PFs are found within 1° and one hour of a
167 hail report, the PF with the coldest minimum 37 GHz PCT is selected as the hail PF.
168 This is because cold 37 GHz PCT has been found related to the large size hail event
169 [Cecil, 2009]. When one PF is collocated with multiple hail reports in U.S., the hail
170 report with the largest hail diameter and the nearest distance from the PF centroid (if
171 more than one hail report is of the maximum hail diameter) is used. In this way, the PF
172 and hail report have a one to one relationship. Note that over China, many hail reports
173 are actually graupel events according to WMO definition. However, to make it easier
174 to describe in the following analysis, we refer them as hail PFs hereafter. To compare
175 the hail PFs with general PFs without hail, in the south-central and southeast U.S.
176 (30.5° – 36.0° N, 105.0° – 80.5° W) PFs not being collocated with any hail report are
177 regarded as non-hail PFs. Because the hail reports are only from weather stations in
178 China (Fig. 1a), only PFs close to stations are considered when we select non-hail PFs.
179 Non-hail PFs in China are defined as those within 1° from weather stations but no hail
180 report within one hour. Note that these criteria probably misidentify some non-hail or
181 hail storms due to the time lags and spatial distances between TRMM overpasses and
182 the hail reports. However, they should provide a decent separation between the hail and
183 non-hail samples.

184

185 Whether hailstones aloft could reach the ground is directly related to the melting time

186 during falling. Given the same maximum hail diameter aloft, it would be easier for hail
187 to reach the surface over elevated terrain due to a shorter distance from the freezing
188 level to ground. This is also the reason for graupel particles being observed frequently
189 over high mountains. For example, the Tibetan Plateau was reported with a high annual
190 hail frequency [Zhang *et al.*, 2008]. Meanwhile, the hail climatology of Ferraro *et al.*
191 [2015] and Cecil and Blankenship [2012] derived from satellite microwave observation
192 show less occurrence of large hail in high altitude regions, especially over the Tibetan
193 Plateau. One reason for this discrepancy is that the hail reports from weather stations
194 over high elevation regions include graupel events with size smaller than 5 mm (Table
195 1). Another factor could be that the satellite measurement favor horizontally extensive
196 storms due to non-uniform beam filling resulting from 4.3 km horizontal resolution
197 (nadir) [Kummerow *et al.*, 1998]. These measurements are suitable for supercells that
198 produce large hail, but not for smaller discrete convective cells that could dump graupel
199 and small hail in a mountainous area. On the contrary, the hail reports in U.S. are
200 dominated by large hail diameter and occur mainly in the Central Plains. To address the
201 differences of hailstorm properties at different elevations, a threshold of 2000 m
202 topography is used to distinguish high elevation and low elevation hail reports and PFs
203 in this study. The TRMM PF centroid location is used to determine the local elevation
204 of PFs and also the corresponding hail reports.

205 **3. Results**

206 **3.1 Locations of hail**

207 The numbers of collocated PFs and hail reports and total hail reports of different hail
208 sizes are listed in Table 1. In China, most hail reports have MHD less than 5 mm, while
209 in U.S. the reported hail diameter is usually ≥ 19.05 mm (the minimum threshold for
210 severe hail before 2010). In U.S., the hail reports number (≥ 19.05 mm) decreases along
211 with the increase of hail size. In China the hail size at low and high elevations have
212 different distributions. Over high elevations, the hail size distribution is close to an
213 exponential distribution and consistent with the observations above freezing level in
214 convective cloud systems over U.S. High Plains [Auer, 1972]. At low elevation, the hail
215 size distribution is close to a gamma distribution which is more consistent with the
216 distribution after melting process of small ice particle [Fraile *et al.*, 2003] (Figures not
217 shown). Compared with the hail size distribution of hail reports at high elevations in
218 China, the fraction of hail size larger than 10 mm is greater in hail reports at low
219 elevations in China, indicating that small hail or graupel are relatively rare at low
220 elevation regions in warm season.

221

222 The locations of hail reports collocated with PFs over China and U.S. are shown in Fig.
223 1. All the collocated hail reports south of 36°N in China are from 118 weather stations
224 (Fig. 1a). The stations with hail reports are mainly located on the Tibetan Plateau where
225 the elevation is above 2000 m. As mentioned earlier, most of the hail reports over Tibet
226 are in fact graupel events. In U.S., the PF collocated with hail reports distribute across

227 the nation in similar pattern of the raw hail reports distribution [*Cecil and Blankenship,*
228 2012]. The collocated hail events are densely distributed in the northern Texas (Fig. 1b),
229 consistent with the distribution of storm data reports and are mainly in the low altitude
230 region, and only a few reports are from over mountains above 2000 m.

231

232 The total number of hail PFs over China at each weather station is shown as symbols
233 of different sizes in Fig 2a. Though there are many weather stations at low elevation
234 regions, not all of them have hail PFs. Over Tibet, however, most of weather stations
235 have multiple hail PFs found during 1998-2013. The observation of interest is to know
236 the fraction of precipitation systems having hail over different regions, in another word,
237 how easy it is to have hail in a precipitation system locally. To answer this question, the
238 fraction of hail PFs at each weather station to total number of PFs within 1° are shown
239 as different colors in Fig. 2a. It is easier to encounter graupel and hail over high
240 mountains. The fraction of hail PFs to all PFs is larger than 0.1% over Tibet, which is
241 ten times larger than many stations at low elevations to the east.

242

243 The number density of hail PFs over the south U.S. is shown as color fill in Fig 2b.
244 Over the south U.S., the fraction is highly related to the PF number spatial distribution.
245 It should be noted that due to the TRMM orbit, a sampling bias of PF numbers exists
246 near 35° . It is quite common to have more than 1% of hail PF fraction over the entire
247 south U.S. The largest fraction reaches 3% in northern Texas, Oklahoma, and some

248 areas in Alabama and Georgia.

249

250 **3.2 Distinctions between hail PFs and Non-hail PFs**

251 To demonstrate the intensity and vertical structure of hail PFs, two dimensional
252 histograms of maximum reflectivity profiles of hail PFs and non-hail PFs over different
253 regions are shown in Fig.3. The distributions of maximum reflectivity profiles have
254 obvious distinctions between hail PFs (Fig. 3a) and non-hail PFs. The maximum
255 reflectivity in low elevation non-hail PFs have a broad distribution from 15 dBZ to 50
256 dBZ in both China and U.S., with maximum frequency around 25 dBZ at 4 km, while
257 the reflectivity of high elevation non-hail PF mainly ranges between 15 dBZ and 35
258 dBZ, with maximum frequency around 7 km above the sea level. Despite of the small
259 sample size of hail PFs over China, low elevation hail PFs in both countries have similar
260 distributions. The maximum frequency centers around 50 dBZ and extends upward to
261 10 km and reflectivity decrease rate is smaller in lower level than in upper level. For
262 high elevation hail PFs in China, the maximum frequency is at 43 dBZ and the
263 reflectivity decreases fast with the height increase.

264

265 The median maximum reflectivity profiles of hail and non-hail PFs in China at high and
266 low elevations and U.S. are further compared in Fig. 4. In general, median maximum
267 reflectivity of non-hail PFs is significantly smaller than that of hail PFs in the two
268 countries and the median maximum reflectivity in U.S. is stronger than that in China.

269 In China, the median maximum reflectivity profiles of hail PFs at high and low
270 elevation are close to each other at altitudes above 8 km. The median maximum
271 reflectivity of non-hail PFs at high elevations is stronger than those at low elevations at
272 altitudes above 6 km. Compared with the radar reflectivity of the deep convection in
273 China [Xu, 2012], the vertical maximum radar reflectivity profiles of hail PFs are close
274 to the PFs in the top 20-30 percentiles. The maximum radar reflectivity in the high
275 elevation region is weaker than those at lower elevation in China. In U.S, the median
276 maximum reflectivity profiles of hail PFs are stronger than those in China. Although
277 the high elevation hail PF in U.S. have weaker reflectivity than low elevation hail PFs
278 below 10 km, they still have close reflectivity intensity above 10 km.

279

280 The standard deviation (SD) of hail PFs and non-hail PFs present evident discrepancies
281 in the amplitude at different altitudes (Fig. 4b). The SD of maximum reflectivity profiles
282 in hail PFs has maximum value above 10 km, indicating great variance in reflectivity
283 of hailstorms at this level. The high reflectivity values and large SD values in the upper
284 troposphere indicate stronger updraft to lift large hailstones to the higher altitudes.
285 Weaker reflectivity in the upper troposphere in hail PFs over China indicates smaller
286 size hail. Small size hail tends to rapidly melt in the melting layer [Rasmussen and
287 Heymsfield, 1987]. Hail diagnosis utilizing single radar data had shown a relation
288 between hail occurrence and the height of the 45 dBZ echo above the freezing level
289 [Mather et al., 1976; Waldvogel et al., 1979]. This is relevant to the larger hail in the

290 U.S. database, more so than the smaller hail in the China database used here. *Donavon*
291 *and Jungbluth* [2007] concluded the strong linear relationship of melting level depth
292 and 50 dBZ echo height for severe hail (>19 mm diameter) producing storms. Strong
293 radar echo at upper troposphere is one important characteristic of hailstorms with large
294 diameter hail.

295

296 To compare the properties of hail and non-hail PFs over China and U.S., the cumulative
297 fraction distribution (CFD) of MIN37PCT, MIN85PCT, maximum reflectivity,
298 TMAXHT30, TMAXHT40, and lightning flash rate are shown Fig. 5. With large ice
299 particles, hail PFs have stronger ice scattering signal, higher radar reflectivity, and more
300 lightning flashes than non-hail PFs. Comparing two regions, hail PFs in U.S. are more
301 intense than China, indicated by lower PCTs (Fig. 5a-b), higher maximum reflectivity
302 (Fig. 5c-e) and lightning flash rates (Fig. 5f). This is consistent with the larger hail
303 diameters in U.S. in Fig. 1. The median minimum 85 GHz brightness temperatures (Fig.
304 5a) are around 178 K for U.S. hail PFs, 224 K for hail PFs from China, and 265 K for
305 non-hail PFs. The median values at 37 GHz (Fig. 5b) are about 252 K for U.S. hail PFs,
306 264 K for hail in China, and 275 K for non-hail PFs. The criteria used for identifying
307 hail in the *Cecil and Blankenship* [*Cecil and Blankenship*, 2012] satellite-based
308 climatology were 200 K at 37 GHz and 130 K at 85 GHz. Only about 15% of the U.S.
309 hail PFs satisfy that criterion at 37 GHz, and only about 27% satisfy that criterion at 85
310 GHz. Almost none of the China hail PFs or the non-hail PFs do. This helps explain the

311 disparity between ground-based climatologies of hail favoring high terrain [*Frisby and*
312 *Sansom, 1967; Williams, 1973*] and satellite-based climatologies almost excluding high
313 terrain. Using such low brightness temperature thresholds puts emphasis on the large
314 hail such as that reported in the U.S. and gives a low overall probability of detection,
315 for the sake of keeping the false alarm rate low.

316

317 Note that about 57.1% (19.8%) of hail PFs do not have 40 dBZ (30 dBZ) in China,
318 compared to 17.0% (6.8%) of hail PFs in the U.S. (Fig. 5c). Because one hour and 1
319 degree criteria give a generous collocation flexibility, these PFs may be falsely
320 identified, or at stages of dissipating or developing of hailstorms. For the large hail
321 reports in U.S., more than 50% of the hail storms have 40 dBZ echo top colder than -
322 20°C, which is considered as the hail growth region [*Browning et al., 1976*]. PFs with
323 lightning flash rate less than 1 flash per minute accounted for around 90% among the
324 entire PFs population, consistent with the results of *Xu [2012]* and *Cecil et al. [2005]*.
325 The fractions of hail PFs having lightning flash rate greater than 1 flash per minute are
326 around 40% and 70% in China and U.S., significantly higher than the non-hail PFs.
327 *Carey et al. [2003]* found 80.7% of the severe storms across the contiguous U.S.,
328 including large hail, strong convective wind, and tornadoes derived from *Storm Data*,
329 occurred along with cloud-to-ground lightning strikes during the warm season. Our
330 results are lower, likely due to the time mismatch between the hail PFs and the real hail
331 events.

332

333 **3.3 Properties of storms with different hail sizes**

334 Previous section has shown remarkable differences in the properties of hail PFs over
335 the two regions. This should be directly related to the distinction in the hail diameters
336 of the two regions (Table 1). This section will depict characteristics of PFs against
337 different hail sizes.

338

339 The relationships between characteristics of hail PFs and hail sizes are presented in the
340 two-dimensional joint histograms (Fig. 6). To separate the cases over the two regions,
341 the histograms are shown in different color-filled contours for China and U.S. Due to
342 the diameter gap in the two countries, the contours distribute in totally different regions.
343 In China, only the high elevation hail PFs are counted in the contour and low elevation
344 hail PFs are scattered in plus signs, among which a few do have large enough diameters
345 to overlap the U.S. histograms.

346

347 It is generally assumed that a large amount of ice particles could lead to passive
348 microwave TB depression in severe convection. *Cecil* [2009] used 180 K at 37 GHz
349 from TRMM as the threshold for large hail and concluded a broad range of TB values
350 for a particular diameter. The wide spread of Minimum 37 GHz and 85GHz PCT are
351 also found in Fig. 6a and 6b. This wide spread of brightness temperatures for a given
352 hail size could be because the brightness temperature reacts to the number concentration

353 and vertical distribution of large particles, in addition to the particle size itself. In
354 addition, due to the coarse thresholds to select PFs, the hail report collocated PFs could
355 be in the developing or dissipation stages before or after hail occurrence, or could
356 include overpasses only partially covering the hailstorm.

357

358 Most of the hail PFs in U.S. have maximum reflectivity around 55 dBZ and hail size
359 around 20 mm, more concentrated in this part of the histogram than the broad
360 distribution of TB. Only a few low elevation hail reports in China have diameter close
361 to 20 mm, which mostly have strong maximum reflectivity exceeding 50 dBZ and are
362 close to those reports with similar hail sizes in U.S. In China, the 40 dBZ echo top
363 temperature of high elevation hail PFs are rarely colder than $-40\text{ }^{\circ}\text{C}$, with frequency
364 maximum around $-15\text{ }^{\circ}\text{C}$. The maxima around $-15\text{ }^{\circ}\text{C}$ is also found in U.S. However,
365 the 40 dBZ echo top temperatures of hail PFs in U.S. distribute over a wider range, as
366 cold as $-60\text{ }^{\circ}\text{C}$. The temperatures of 30 dBZ echo top show maximum around $-20\text{ }^{\circ}\text{C}$
367 and $-60\text{ }^{\circ}\text{C}$ in China and U.S., respectively. Fig. 6e also suggests that 30 dBZ echo top
368 temperature might be used as an indicator of the hail size, since there is a good
369 separation of the hail sizes in PFs of different 30 dBZ echo top temperatures in general,
370 including those over high terrain. The histogram of lightning flash rates in hail PFs span
371 a wide range of values for a specific hail size, in U.S. (Fig. 6f), though it is also clear
372 that hailstorms with larger hail sizes tend to have higher flash rates.

373

374 Percentages of hail PF with different hail size are calculated and shown in Fig. 7. In
375 general, percentages tend to rise with the decrease of minimum 85 (37) GHz PCT,
376 maximum 30 and 40 dBZ echo top height (lower echo top temperature) and the increase
377 of maximum reflectivity and lightning flash rate in both countries. Over China, the
378 percentages of hail PFs are much smaller than those over U.S., likely due to the China
379 database being restricted to fixed observing locations. Therefore a different scale is used.
380

381 In the U.S. database, any given brightness temperature (Fig. 7 a-b), maximum
382 reflectivity value (Fig. 7c), or lightning flash rate (Fig. 7f) has a greater likelihood of
383 the smaller hail category (10-30 mm) than either of the larger hail categories. But more
384 than half the overall U.S. hail database is comprised of these 10-30 mm diameter reports
385 (Table 1). The larger hail sizes do become more predominant with 40 dBZ echo tops
386 colder than -60° C (Fig. 7d). The sample sizes do become small for the coldest echo
387 tops, and the decrease in overall probabilities for the coldest values might not be
388 meaningful. The total probability of any hail 10 mm or larger (adding the values of the
389 blue lines in Fig. 7) is consistent with values reported by *Cecil and Blankenship* [2012].
390 Whereas *Cecil* [2009] and *Cecil and Blankenship* [2012] found that the probability of
391 hail occurrence is better constrained by 37 GHz PCT than by 85 GHz PCT, Fig. 7 shows
392 that stratifying by 37 GHz PCT yields higher hail probabilities than any of the other
393 parameters considered here.

394

395 In China, the percentages are much smaller than those of U.S. due to the limited hail
396 reports resources, but the hail probability still increases as the PF intensity increases.
397 For the small hail (graupel) cases in China, percentages peak in relatively weaker PFs,
398 as indicated by the intensity proxies. For example, those small hail (graupel)
399 probabilities peak around 195 K for 85 GHz PCT, 245 K for 37 GHz PCT, 44 dBZ for
400 maximum reflectivity, -25 °C for TMAXHT40, -45 °C for TMAXHT30, and lightning
401 flash rates below 10 flashes per minute. The percentages for hailstorms with larger (5-
402 10 mm) size maintain a constant increase with more intense PFs. In addition, for
403 hailstorms with hail size larger than 5 mm, the percentages increase rapidly when the
404 maximum 40 dBZ echo top temperature is colder than -20 °C, especially for hail size
405 between 5-30 mm.

406

407 To examine the reflectivity profiles of PFs with different hail sizes, the median
408 maximum reflectivity profiles of hail PFs are categorized against maximum hail
409 diameter (Fig. 8). Reflectivity profiles of Chinese hail PFs at low elevations have large
410 variability due to the limited collocated PF number, especially for hail PFs with size
411 larger than 5 mm, but still have remarkable results. PFs with graupel (hail size < 5 mm)
412 have about 5 dB smaller maximum reflectivity than those with 5-10 mm hail size at all
413 levels. The profile of low elevation PFs with hail size greater than 10 mm in China is
414 close to profiles in U.S. in low levels. This provides some confidence for the consistent
415 properties of hailstorms over the two regions, when considering similar hail sizes.

416

417 Larger hail diameters in low elevation are associated with larger median maximum
418 reflectivity at altitudes above 6 km, and with higher the echo tops. However, at altitudes
419 below 5 km, only small differences (< 3 dB) are found between the hail size categories
420 from the U.S. There are several reasons to be skeptical about the radar data at the lower
421 altitudes. The downward-looking Ku-band TRMM radar is subject to increasing
422 attenuation as one progresses to lower altitudes, especially for the types of storms we
423 are considering here, with large particles aloft. A standard attenuation correction is
424 applied, but considerable uncertainty remains. Multiple scattering effects in a hailstorm
425 complicate interpretation of the radar reflectivity [Battaglia *et al.*, 2015]. Non-uniform
426 beam filling and the mixture of hail with large raindrops within a sample volume are
427 also concerns. Small hail often reaches the surface accompanied by large raindrops
428 from melted hail, with those particles having fairly similar terminal velocities. Larger
429 hail often reaches the surface in the absence of raindrops, with the hail stones falling
430 through an updraft that is strong enough to suspend the rain drops aloft. Storm evolution
431 during the one-hour time window we allow for matching PFs with hail reports must
432 also be considered. In modeling hail size with a one dimensional model [Brimelow *et*
433 *al.*, 2002], hailstone growth time in the cloud ranged from 40 minutes to more than 60
434 minutes before reaching the ground. The TRMM measurements that observed the cloud
435 aloft could be biased towards including times when hail is actually present aloft, but
436 not reaching the ground.

437

438 For the hail PFs at high elevations, there is a clear separation between the reflectivity
439 profiles as a function of hail diameter. However, the maximum reflectivity profiles of
440 high elevation hail PFs (> 10 mm for China and all hail PFs in U.S.) are close, indicating
441 the possible identity of hailstorm structures in the two regions. The maximum values of
442 the reflectivity profiles are consistently smaller than the ones associated with the same
443 hail diameters at lower elevations. The "typical" storm delivering small hail or graupel
444 (< 5 mm diameter) to the surface at low elevations has about 45 dBZ at 2 km and 40
445 dBZ at 6 km in Fig. 8. This small hail or graupel may be mixed with rain from melted
446 hail, and there are likely larger ice particles aloft that partially melt during their fall. A
447 similar 40 dBZ echo at 6 km altitude would be consistent with somewhat larger hail
448 (~10 mm) reaching the surface if over high terrain. The typical storm producing graupel
449 at the surface over high terrain has only 30-35 dBZ at 6-7 km altitude, and the graupel
450 would likely melt entirely before reaching the surface if located over lower terrain.

451

452 **4. Summary**

453 After collocating a 16-year record of TRMM precipitation features with ground hail
454 reports, the properties of hailstorms in China and the U.S. are discussed. Two countries
455 reports different ranges of ground hail sizes in general. However, this provides a unique
456 opportunity to study properties of hailstorms with different hail sizes at different
457 elevations using uniform satellite observations. The major conclusions are listed as

458 follow.

459 ● Due to the different methods of reporting hail and the different characteristics
460 of storms over the two regions, the hail reports differ greatly between the two
461 countries. Hail events reported in China tend to have smaller diameter than
462 those in the U.S. The diameters reported in China are mostly between 1-10 mm
463 (this includes graupel), but the U.S. rarely collects reports of hail smaller than
464 19 mm. The China hail reports are from fixed meteorological observing sites,
465 but the U.S. hail reports are culled from members of the public who describe
466 the largest hail encountered at their locations. The number of hail reports and
467 the fraction of precipitation systems accompanied by hail based on these
468 present datasets is almost two orders of magnitude higher in the south U.S. than
469 in China. For the hail reports used in this study, about 89% of the hail and
470 graupel reports from China are at high elevations, while about 99% of the U.S.
471 reports are from lower elevations.

472 ● By combining the small hail reports in China and large hail reports in U.S., the
473 remote sensing properties of hailstorms with a full spectra of hail sizes are
474 examined for the first time. The hailstorms reported in the U.S., dominated by
475 large hail, are generally stronger than those storms with small hail sizes in
476 China, with higher radar reflectivity, higher lightning flash rate, and lower
477 passive microwave brightness temperatures. Though in general, storms with
478 larger hail sizes are more intense, the storms with larger hail sizes tend to have

479 very broad ranges of values for most parameters studied here.

480 ● The maximum reflectivity profiles of storms show stronger reflectivity as the
481 hail size increases. Radar reflectivity tends to be larger at levels above 6 km for
482 storms with larger hail sizes. This is consistent with larger hail size ice particles
483 at high elevations. However, TRMM PR shows similar maximum radar
484 reflectivity values below the freezing level in storms regardless of hail size.
485 There are many reasons to be wary of interpreting the TRMM radar reflectivity
486 at low levels in intense storms. In high elevation regions, the graupel and hail
487 reports are from storms with relatively weaker convective intensity.

488 ● In this study, we have demonstrated that in the overlapped hail size range, the
489 systems over China and U.S. have close radar reflectivity and passive
490 microwave TB properties (Figure 3, Figure 6, and Figure 8). This indicates that
491 storms with similar hail sizes over different regions share similar remote
492 sensing properties. However, the hail events are not reported in same way in
493 two countries, there could be arguments that small hail events (ice particles <
494 0.75 inch) in U.S. being different from those in China, and there is no way to
495 validate that yet since the graupel events are not reported in U.S.; or, the
496 systems containing the largest hail sizes over China could be different from
497 those over U.S. All these need further validations when more relevant
498 observations become available.

499 **Acknowledgement**

500 This study is supported by the Chinese National Science Foundation under Grants
501 41330421 and 41461164006 and by the NASA Precipitation Measurement Missions
502 Science Team. The first author gratefully acknowledge the financial support from the
503 China Scholarship Council. The TRMM Precipitation Feature Database could be
504 obtained freely from <http://atmos.tamucc.edu/trmm/>. The hail reports in U. S. are
505 updated by NCDC (<http://www1.ncdc.noaa.gov/pub/data/swdi/stormevents/csvfiles/>).
506 Due to the National data management policy, the use of station hail size records in China
507 must be authorized by the Meteorological Information Center of the China
508 Meteorological Administration (<http://www.nmic.gov.cn/web/index.htm>).
509

510 **Figure Caption**

511 Fig. 1. (a) Locations of stations with collocated hail reports and TRMM Precipitation
512 Features in China. For each station, the mean values of reported maximum hail diameter
513 (MHD) at each station are marked with different symbols in this figure; (b) Locations
514 of collocated hail reports with the reported hail diameter in United States. The bold
515 solid lines are the contour lines at 2000 m.

516 Fig. 2. (a) The symbols indicate the number of graupel and hail reports collocated with
517 precipitation features (PFs) and the color represents the fraction of collocated PFs
518 number to all PFs number at each stations; (b) The filled blue shading is the hail PFs
519 number, and the red color contours are percentage of hail PFs relative to all PFs number,
520 with contour levels 1%, 2%, 3%. The contoured data are calculated in 1° by 1° grid
521 cells. In (a) and (b), the bold solid lines are 2000 m contour line.

522 Fig. 3. Two dimensional histogram of maximum reflectivity profiles of low elevation
523 hail precipitation features (PFs) in China (a); low elevation non-hail PFs in China (b);
524 high elevation hail PFs in China (c); high elevation non-hail PFs in China (d); low
525 elevation hail PFs in U.S. (e); and low elevation non-hail PFs in U.S. (f). The three lines
526 are reflectivity at 25th, 50th, and 75th percentiles at each level. Note that reflectivity
527 below 15 dBZ, including 0 dBZ, are all utilized in the calculation of percentiles.

528 Fig. 4. The median maximum reflectivity profiles of non-hail precipitation feature (a)
529 and corresponding standard deviation profiles (b).

530 Fig. 5. The cumulative fractions of minimum 85 GHz PCT (a), minimum 37 GHz PCT

531 (b), maximum reflectivity of MAXDBZ profiles (c), maximum 40 dBZ echo top
532 temperature (d), maximum 30 dBZ echo top temperature (e), and lightning flash rate (f)
533 of Non-hail Precipitation Features (PFs) and Hail PFs in China and US.

534 Fig. 6. Two-dimensional histograms of properties of hail precipitation features against
535 hail sizes. a) minimum 85 GHz PCT; b) minimum 37 GHz PCT; c) maximum radar
536 reflectivity at any level; d) maximum 40 dBZ echo top temperature; e) maximum 30
537 dBZ echo top temperature; f) lightning flash rate. The histograms of US hail PFs are
538 shown in red contours and China shown in blue color-filled contours. The scattered plus
539 signs are the hail PFs at low elevation (<2000 m) in China.

540 Fig. 7. Percentage of Hail Precipitation Features (PF) relative to all PF, for different hail
541 sizes. Percentages are calculated in bins centered the markers for a) minimum 85 GHz
542 PCT; b) minimum 37 GHz PCT; c) maximum radar reflectivity at any level; d)
543 maximum 40 dBZ echo top temperature; e) maximum 30 dBZ echo top temperature; f)
544 lightning flash rate. As the percentages of hail PFs in China are much smaller than those
545 in U.S., different vertical coordinates are utilized in each subplot.

546 Fig. 8. The median maximum reflectivity profiles of hail Precipitation Features with
547 different maximum hail diameter (MHD) at high elevation (High) and low elevation
548 (Low).

549

550 **Reference**

- 551 Allen, J. T., and M. K. Tippett (2015), The Characteristics of United States Hail
552 Reports : 1955 – 2014, *Electron. J. Sev. Storms Meteorol.*, *10*(3), 1–31.
- 553 Auer, A. (1972), Distribution of graupel and hail with size, *Mon. Weather Rev.*,
554 *100*(5), 325–328, doi:10.1175/1520-0493-100-05-0325.
- 555 Battaglia, A., S. Tanelli, K. Mroz, and F. Tridon (2015), Multiple scattering in
556 observations of the GPM dual-frequency precipitation radar: evidence and
557 impact on retrievals, *J. Geophys. Res. Atmos.*, 4090–4101,
558 doi:10.1002/2014JD022866.
- 559 Berthet, C., J. Dessens, and J. L. Sanchez (2011), Regional and yearly variations of
560 hail frequency and intensity in France, *Atmos. Res.*, *100*(4), 391–400,
561 doi:10.1016/j.atmosres.2010.10.008.
- 562 Brimelow, J. C., G. W. Reuter, and E. R. Poolman (2002), Modeling Maximum Hail
563 Size in Alberta Thunderstorms, *Weather Forecast.*, *17*(5), 1048–1062,
564 doi:10.1175/1520-0434(2002)017<1048:MMHSIA>2.0.CO;2.
- 565 Browning, K. A., J. C. Frankhauser, J. P. Chalon, P. J. Eccles, R. G. Strauch, F. H.
566 Merrem, D. J. Musil, E. L. May, and W. R. Sand (1976), Structure of an evolving
567 hailstorm part V: Synthesis and implications for hail growth and hail
568 suppression, *Mon. Weather Rev.*, *104*(5), 603–610, doi:10.1175/1520-
569 0493(1976)104<0603:SOAEHP>2.0.CO;2.
- 570 Carey, L. D., S. A. Rutledge, and W. A. Petersen (2003), The relationship between

571 severe storm reports and cloud-to-ground lightning polarity in the contiguous
572 United States from 1989 to 1998, *Mon. Weather Rev.*, 131(7), 1211–1228,
573 doi:10.1175/1520-0493(2003)131<1211:TRBSSR>2.0.CO;2.

574 Cecil, D. J. (2009), Passive Microwave Brightness Temperatures as Proxies for
575 Hailstorms, *J. Appl. Meteorol. Climatol.*, 48(6), 1281–1286,
576 doi:10.1175/2009JAMC2125.1.

577 Cecil, D. J. (2011), Relating passive 37-GHz scattering to radar profiles in strong
578 convection, *J. Appl. Meteorol. Climatol.*, 50(1), 233–240,
579 doi:10.1175/2010JAMC2506.1.

580 Cecil, D. J., and C. B. Blankenship (2012), Toward a Global Climatology of Severe
581 Hailstorms as Estimated by Satellite Passive Microwave Imagers, *J. Clim.*, 25(2),
582 687–703, doi:10.1175/JCLI-D-11-00130.1.

583 Cecil, D. J., S. J. Goodman, D. J. Boccippio, E. J. Zipser, and S. W. Nesbitt (2005),
584 Three Years of TRMM Precipitation Features. Part I: Radar, Radiometric, and
585 Lightning Characteristics, *Mon. Weather Rev.*, 133(3), 543–566,
586 doi:10.1175/MWR-2876.1.

587 Changnon, S. A., and D. Changnon (2000), Long-Term Fluctuations in Hail
588 Incidences in the United States, *J. Clim.*, 13, 658–664, doi:10.1175/1520-
589 0442(2000)013<0658:LTFIHI>2.0.CO;2.

590 Changnon, S. A., D. Changnon, and S. D. Hilberg (2009), *Hailstorms across the*
591 *nation: An atlas about hail and its damages*. Illinois State Water Survey Contract

592 Report 2009-12, 64-65.

593 Cintineo, J. L., T. M. Smith, V. Lakshmanan, H. E. Brooks, and K. L. Ortega (2012),
594 An Objective High-Resolution Hail Climatology of the Contiguous United
595 States, *Weather Forecast.*, 27(5), 1235–1248, doi:10.1175/WAF-D-11-00151.1.

596 Dee, D. P. et al. (2011), The ERA-Interim reanalysis: Configuration and performance
597 of the data assimilation system, *Q. J. R. Meteorol. Soc.*, 137(656), 553–597,
598 doi:10.1002/qj.828.

599 Deierling, W., and W. A. Petersen (2008), Total lightning activity as an indicator of
600 updraft characteristics, *J. Geophys. Res. Atmos.*, 113(16),
601 doi:10.1029/2007JD009598.

602 Dobur, J. C. (2005), A comparison of severe thunderstorm warning verification
603 statistics and population density within the NWS Atlanta county warning area,

604 Donavon, R. a., and K. a. Jungbluth (2007), Evaluation of a Technique for Radar
605 Identification of Large Hail across the Upper Midwest and Central Plains of the
606 United States, *Weather Forecast.*, 22(2), 244–254, doi:10.1175/WAF1008.1.

607 Ferraro, R., J. Beauchamp, D. Cecil, and G. Heymsfield (2015), A prototype hail
608 detection algorithm and hail climatology developed with the advanced
609 microwave sounding unit (AMSU), *Atmos. Res.*, 163, 24–35,
610 doi:10.1016/j.atmosres.2014.08.010.

611 Fraile, R., A. Castro, L. López, J. L. Sánchez, and C. Palencia (2003), The influence
612 of melting on hailstone size distribution, *Atmos. Res.*, 67-68, 203–213,

613 doi:10.1016/S0169-8095(03)00052-8.

614 Frisby, E. M., and H. W. Sansom (1967), Hail Incidence in the Tropics, *J. Appl.*
615 *Meteorol.*, 6(2), 339–354, doi:10.1175/1520-
616 0450(1967)006<0339:HIITT>2.0.CO;2.

617 Gallo, K., T. Smith, K. Jungbluth, and P. Schumacher (2012), Hail Swaths Observed
618 from Satellite Data and Their Relation to Radar and Surface-Based Observations:
619 A Case Study from Iowa in 2009, *Weather Forecast.*, 27(3), 796–802,
620 doi:10.1175/WAF-D-11-00118.1.

621 Hamada, A., Y. N. Takayabu, C. Liu, and E. J. Zipser (2015), Weak linkage between
622 the heaviest rainfall and tallest storms, *Nat. Commun.*, 6, 6213,
623 doi:10.1038/ncomms7213.

624 Heinselman, P. L., and A. V. Ryzhkov (2006), Validation of Polarimetric Hail
625 Detection, *Weather Forecast.*, 21(5), 839–850, doi:10.1175/WAF956.1.

626 Iguchi, T., T. Kozu, R. Meneghini, J. Awaka, and K. Okamoto (2000), Rain-Profiling
627 Algorithm for the TRMM Precipitation Radar, *J. Appl. Meteorol.*, 39(12), 2038–
628 2052, doi:10.1175/1520-0450(2001)040<2038:RPAFTT>2.0.CO;2.

629 Iguchi, T., T. Kozu, J. Kwiatkowski, R. Meneghini, J. Awaka, and K. Okamoto
630 (2009), Uncertainties in the Rain Profiling Algorithm for the TRMM
631 Precipitation Radar, *J. Meteorol. Soc. Japan*, 87A, 1–30,
632 doi:10.2151/jmsj.87A.1.

633 Jirak, I. L., W. R. Cotton, and R. L. McAnelly (2003), Satellite and Radar Survey of

634 Mesoscale Convective System Development, *Mon. Weather Rev.*, *131*(10),
635 2428–2449, doi:10.1175/1520-0493(2003)131<2428:SARSOM>2.0.CO;2.

636 Kim, C., and X. Ni (2015), Climatology of Hail in North Korea (in Chinese), *Acta Sci.*
637 *Nat. Univ. Pekin.*, *51*(3), 437–443, doi:10.13209/j.0479-8023.2014.136.

638 Knight, C. A., and N. C. Knight (2001), *Severe Convective Storms*, edited by D. C. A.
639 D. III, American Meteorological Society.

640 Kummerow, C., W. Barnes, T. Kozu, J. Shiue, and J. Simpson (1998), The Tropical
641 Rainfall Measuring Mission (TRMM) sensor package, *J. Atmos. Ocean.*
642 *Technol.*, *15*(3), 809–817, doi:10.1016/0273-1177(94)90210-0.

643 Liu, C., and E. J. Zipser (2005), Global distribution of convection penetrating the
644 tropical tropopause, *J. Geophys. Res. Atmos.*, *110*(23), 1–12,
645 doi:10.1029/2005JD006063.

646 Liu, C., E. J. Zipser, D. J. Cecil, S. W. Nesbitt, and S. Sherwood (2008), A cloud and
647 precipitation feature database from nine years of TRMM observations, *J. Appl.*
648 *Meteorol. Climatol.*, *47*(10), 2712–2728, doi:10.1175/2008JAMC1890.1.

649 Manzato, A. (2012), Hail in Northeast Italy: Climatology and Bivariate Analysis with
650 the Sounding-Derived Indices, *J. Appl. Meteorol. Climatol.*, *51*(3), 449–467,
651 doi:10.1175/JAMC-D-10-05012.1.

652 Mather, G. K., D. Treddenick, and R. Parsons (1976), An Observed Relationship
653 between the Height of the 45 dBZ Contours in Storm Profiles and Surface Hail
654 Reports, *J. Appl. Meteorol.*, *15*(12), 1336–1340, doi:10.1175/1520-

655 0450(1976)015<1336:AORBTH>2.0.CO;2.

656 Nesbitt, S. W., and E. J. Zipser (2000), A census of precipitation features in the
657 tropics using TRMM: Radar, ice scattering, and lightning observations, *J. Clim.*,
658 *13*(23), 4087–4106, doi:10.1175/1520-0442(2000)013<4087:ACOPFI>2.0.CO;2.

659 Ortega, K. L., T. M. Smith, K. L. Manross, K. A. Scharfenberg, W. Arthur, A. G.
660 Kolodziej, and J. J. Gourley (2009), The severe hazards analysis and verification
661 experiment, *Bull. Am. Meteorol. Soc.*, *90*(10), 1519–1530,
662 doi:10.1175/2009BAMS2815.1.

663 Ortega, K. L., J. M. Krause, and A. V. Ryzhkov (2016), Polarimetric radar
664 characteristics of melting hail. Part III: Validation of the algorithm for hail size
665 discrimination., *J. Appl. Meteorol. Climatol.*, 160203133521006,
666 doi:10.1175/JAMC-D-15-0203.1.

667 Rasmussen, R. M., and A. J. Heymsfield (1987), Melting and Shedding of Graupel
668 and Hail. Part 2: Sensitivity Study, *J. Atmos. Sci.*, *44*(19), 2764–2782,
669 doi:10.1175/1520-0469(1987)044<2754:MASOGA>2.0.CO;2.

670 Schaefer, J. T., and R. Edwards (1999), The SPC Tornado/Severe Thunderstorm
671 Database, Preprints, in *11th Conf. Applied Climatology*, Dallas, TX, US.

672 Schaefer, J. T., J. J. Levit, S. J. Weiss, and D. W. McCarthy (2004), The Frequency of
673 Large Hail Over the Contiguous United States, in *14th Conf. Applied
674 Climatology*, Seattle US.

675 Spencer, J. R., L. A. Lebofsky, and M. V. Sykes (1989), Systematic biases in

676 radiometric diameter determinations, *Icarus*, 78(2), 337–354, doi:10.1016/0019-
677 1035(89)90182-6.

678 Tuovinen, J.-P., A.-J. Punkka, J. Rauhala, H. Hohti, and D. M. Schultz (2009),
679 Climatology of Severe Hail in Finland: 1930–2006, *Mon. Weather Rev.*, 137(7),
680 2238–2249, doi:10.1175/2008MWR2707.1.

681 Vinet, F. (2000), Climatology of hail in France, *Atmos. Res.*, 56(1-4), 309–323,
682 doi:10.1016/S0169-8095(00)00082-X.

683 Waldvogel, A., B. Federer, and P. Grimm (1979), Criteria for the Detection of Hail
684 Cells, *J. Appl. Meteorol.*, 18, 1521–1525, doi:10.1175/1520-
685 0450(1979)018<1521:CFTDOH>2.0.CO;2.

686 Williams, L. (1973), *Hail and its distribution*. Study of the Army Aviation (V/STOL
687 Environment), Army Engineer Topographic Laboratories Rep.8, ETL-SR73-3,
688 27 pp.

689 Witt, A., M. D. Eilts, G. J. Stumpf, E. D. W. Mitchell, J. T. Johnson, and K. W.
690 Thomas (1998), Evaluating the Performance of WSR-88D Severe Storm
691 Detection Algorithms, *Weather Forecast.*, 13(2), 513–518, doi:10.1175/1520-
692 0434(1998)013<0513:ETPOWS>2.0.CO;2.

693 Xie, B., Q. Zhang, and Y. Wang (2008), Trends in hail in China during 1960–2005,
694 *Geophys. Res. Lett.*, 35(13), L13801, doi:10.1029/2008GL034067.

695 Xie, B., Q. Zhang, and Y. Wang (2010), Observed Characteristics of Hail Size in Four
696 Regions in China during 1980–2005., *J. Clim.*, 23(18), 4973–4982,

697 doi:10.1175/2010JCLI3600.1.

698 Xu, W. (2012), Precipitation and Convective Characteristics of Summer Deep
699 Convection over East Asia Observed by TRMM, *Mon. Weather Rev.*, (2012),
700 121114113537007, doi:10.1175/MWR-D-12-00177.1.

701 Zhang, C., Q. Zhang, and Y. Wang (2008), Climatology of Hail in China: 1961–2005,
702 *J. Appl. Meteorol. Climatol.*, 47(3), 795–804, doi:10.1175/2007JAMC1603.1.

703 Zipser, E. J., D. J. Cecil, C. Liu, S. W. Nesbitt, and D. P. Yorty (2006), Where are the
704 most: Intense thunderstorms on Earth?, *Bull. Am. Meteorol. Soc.*, 87(8), 1057–
705 1071, doi:10.1175/BAMS-87-8-1057.

706

707 **Tables**

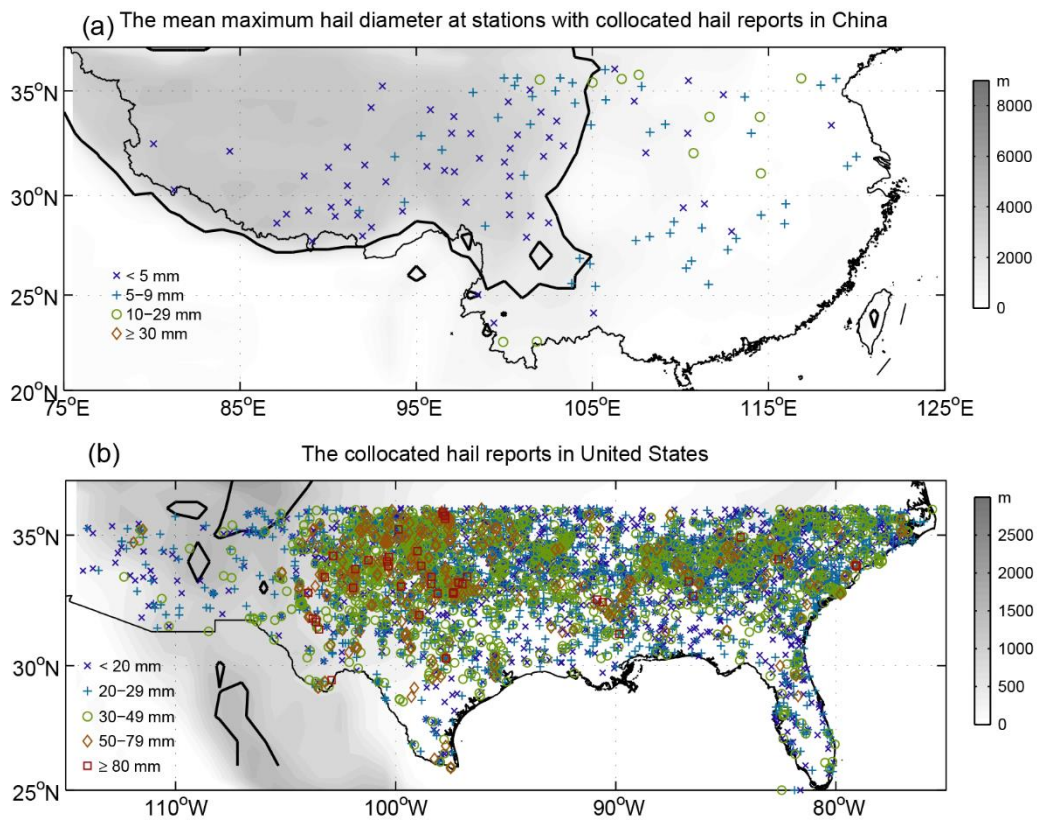
708 Table 1. Collocated hail numbers and all hail reports in different hail size intervals in

709 China and United States south of 36°N.

Diameter (mm)	China				U.S.			
	High elevation (≥2000 m)		Low elevation (<2000m)		High elevation (≥2000 m)		Low elevation (<2000m)	
	All	Collocated	All	Collocated	All	Collocated	All	Collocated
<5	4318	445	199	17	0	0	0	0
5-9	1409	180	362	40	0	0	10	2
10-29	189	17	154	12	532	39	45123	4677
30-49	15	3	23	1	202	6	13668	1472
50-79	0	0	6	0	51	0	2917	38
≥80	0	0	0	0	6	0	333	41

710

711 **Figures**



712

713 Fig. 1. (a) Locations of stations with collocated hail reports and TRMM Precipitation

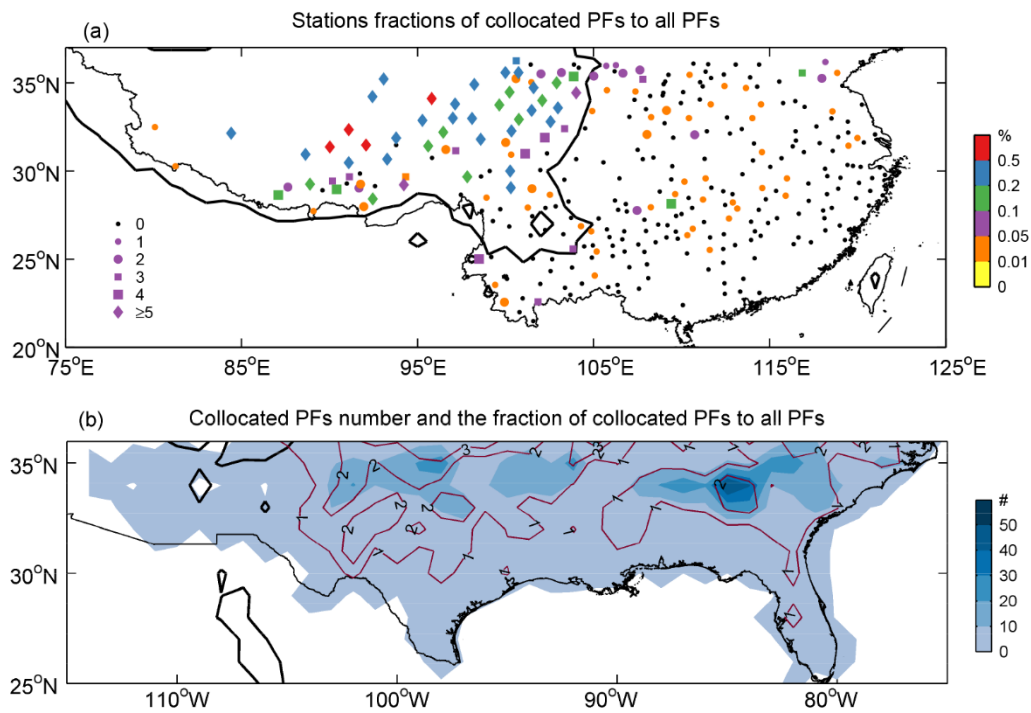
714 Features in China. For each station, the mean values of reported maximum hail diameter

715 (MHD) at each station are marked with different symbols in this figure; (b) Locations

716 of collocated hail reports with the reported hail diameter in United States. The bold

717 solid lines are the contour lines at 2000 m.

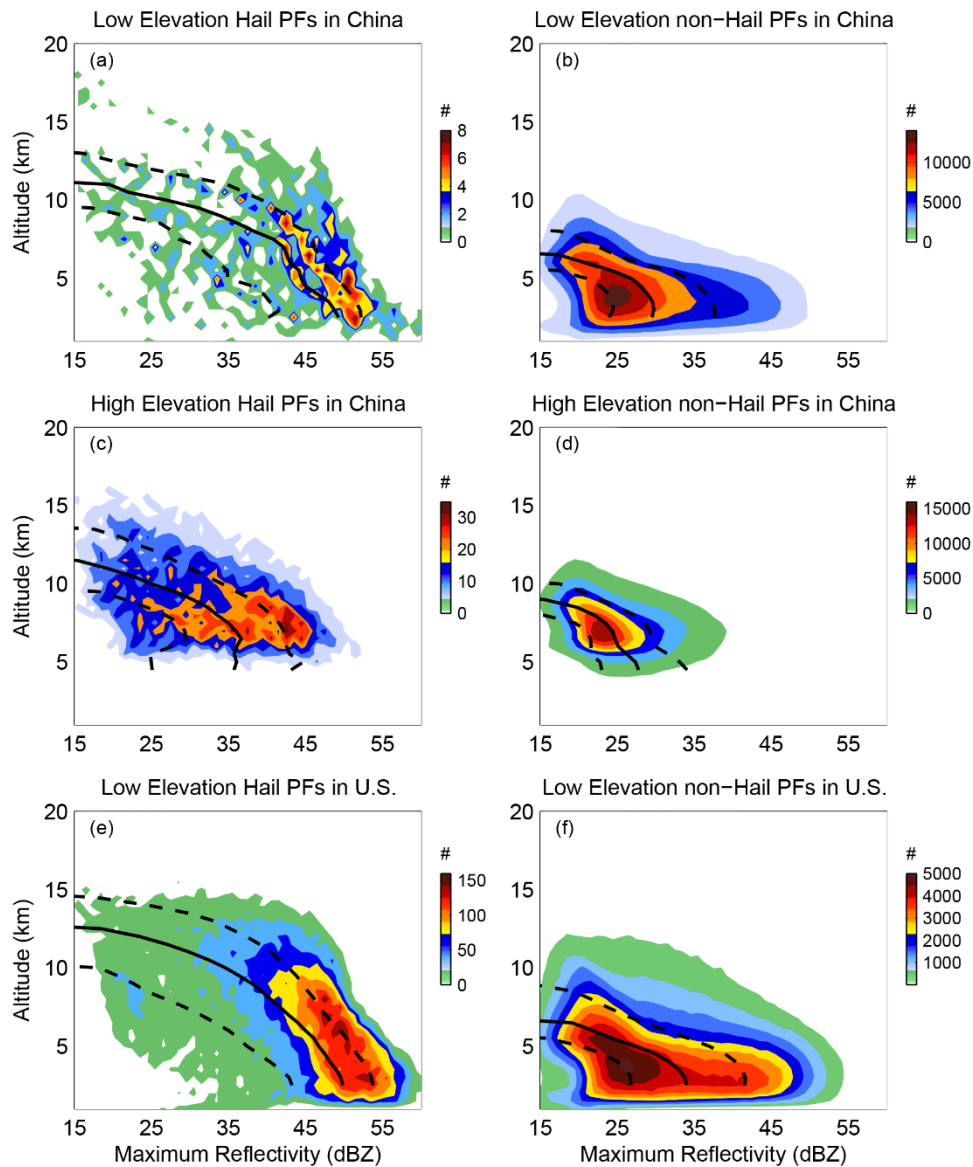
718



719

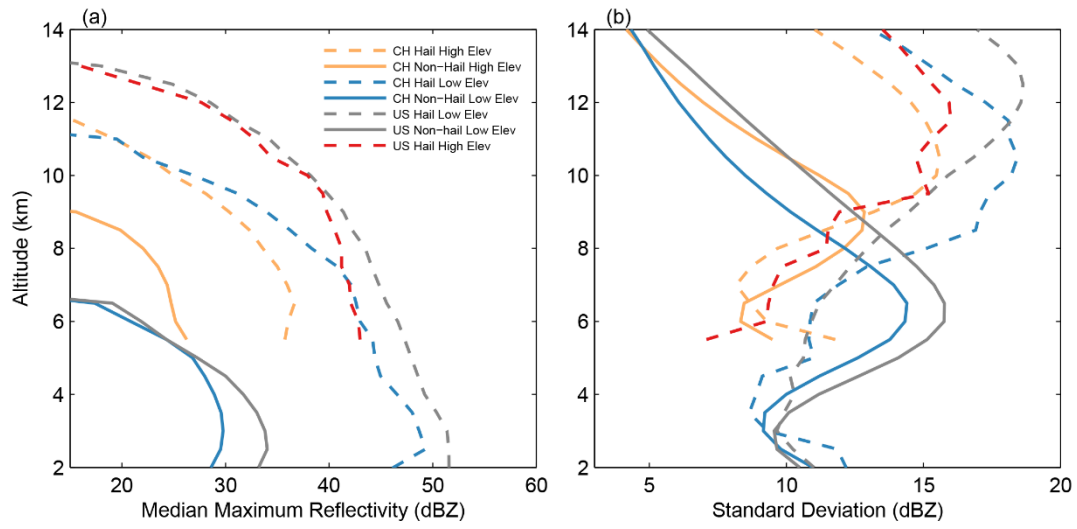
720 Fig. 2. (a) The symbols indicate the number of graupel and hail reports collocated with
 721 precipitation features (PFs) and the color represents the fraction of collocated PFs
 722 number to all PFs number at each stations; (b) The filled blue shading is the hail PFs
 723 number, and the red color contours are percentage of hail PFs relative to all PFs number,
 724 with contour levels 1%, 2%, 3%. The contoured data are calculated in 1° by 1° grid
 725 cells. In (a) and (b), the bold solid lines are 2000 m contour line.

726



727

728 Fig. 3. Two dimensional histogram of maximum reflectivity profiles of low elevation
 729 hail precipitation features (PFs) in China (a); low elevation non-hail PFs in China (b);
 730 high elevation hail PFs in China (c); high elevation non-hail PFs in China (d); low
 731 elevation hail PFs in U.S. (e); and low elevation non-hail PFs in U.S. (f). The three
 732 lines are reflectivity at 25th, 50th, and 75th percentiles at each level. Note that
 733 reflectivity below 15 dBZ, including 0 dBZ, are all utilized in the calculation of
 734 percentiles.

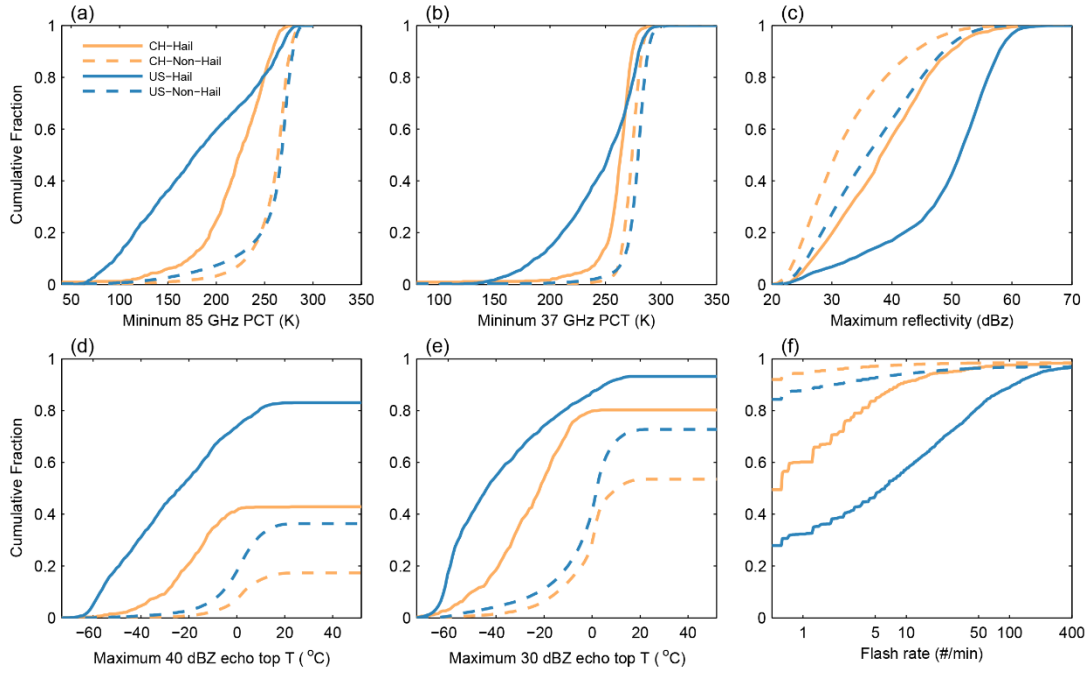


735

736 Fig. 4. The median maximum reflectivity profiles of non-hail precipitation feature (a)

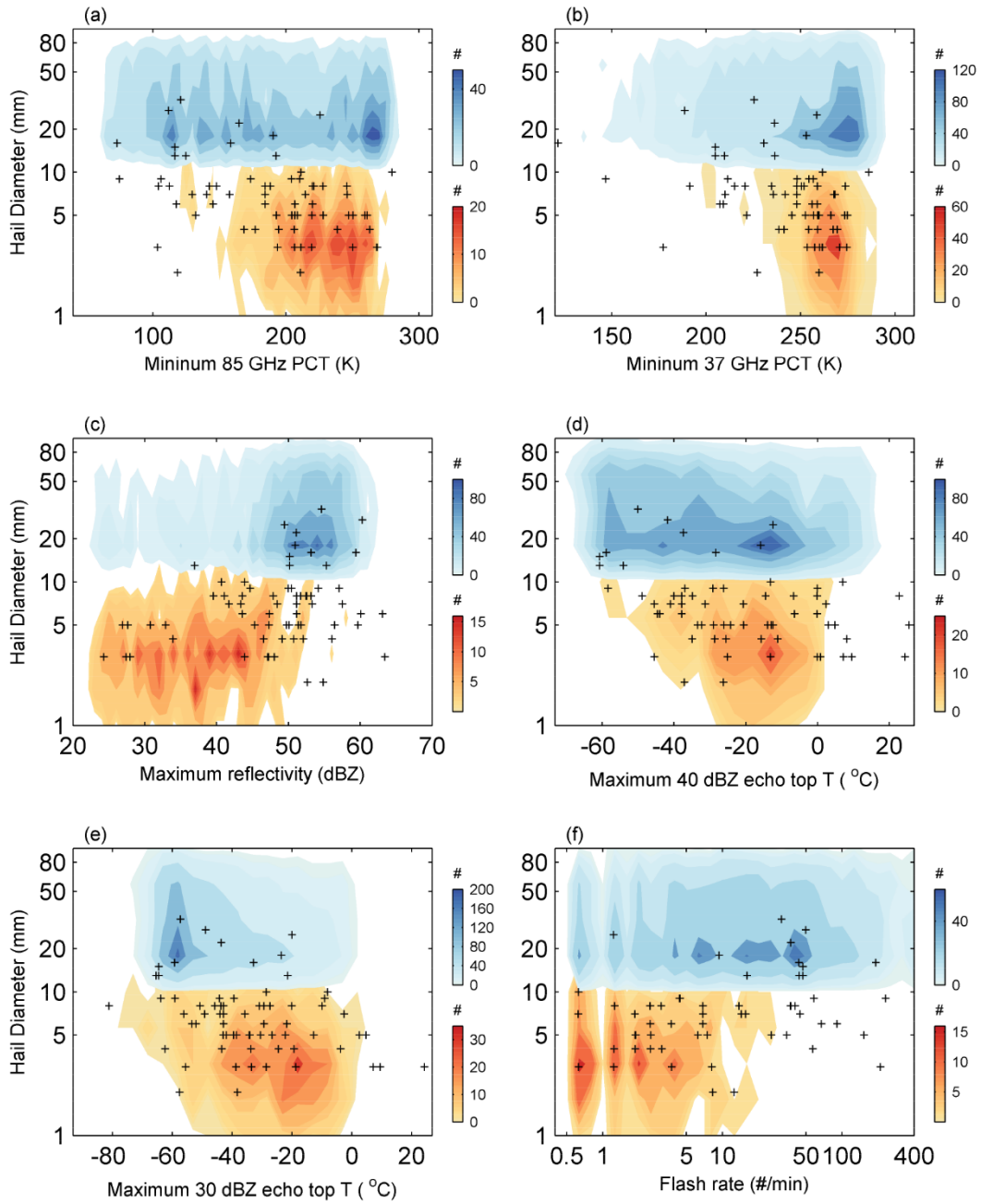
737 and corresponding standard deviation profiles (b).

738



739

740 Fig. 5. The cumulative fractions of minimum 85 GHz PCT (a), minimum 37 GHz PCT
 741 (b), maximum reflectivity of MAXDBZ profiles (c), maximum 40 dBZ echo top
 742 temperature (d), maximum 30 dBZ echo top temperature (e), and lightning flash rate (f)
 743 of Non-hail Precipitation Features (PFs) and Hail PFs in China and US.



744

745 Fig. 6. Two-dimensional histograms of properties of hail precipitation features against

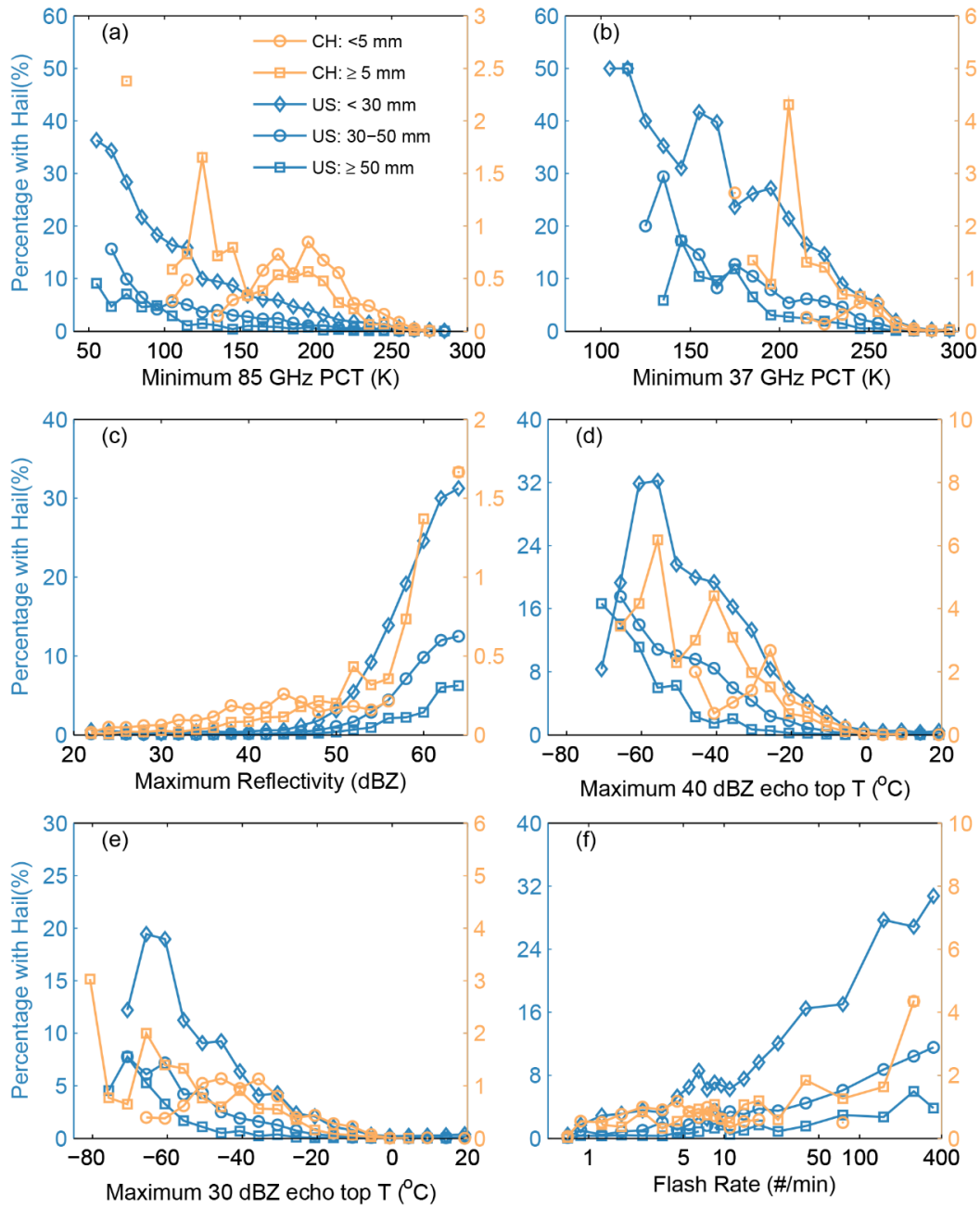
746 hail sizes. a) minimum 85 GHz PCT; b) minimum 37 GHz PCT; c) maximum radar

747 reflectivity at any level; d) maximum 40 dBZ echo top temperature; e) maximum 30

748 dBZ echo top temperature; f) lightning flash rate. The histograms of US hail PFs are

749 shown in red contours and China shown in blue color-filled contours. The scattered plus

750 signs are the hail PFs at low elevation (<2000 m) in China.



751

752 Fig. 7. Percentage of Hail Precipitation Features (PF) relative to all PF, for different hail

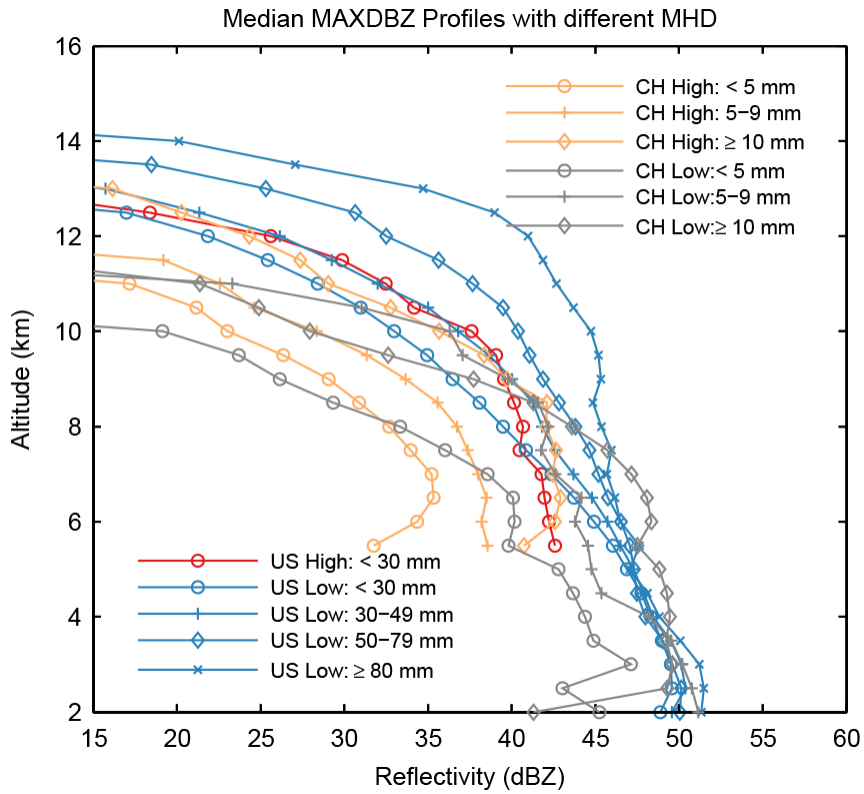
753 sizes. Percentages are calculated in bins centered the markers for a) minimum 85 GHz

754 PCT; b) minimum 37 GHz PCT; c) maximum radar reflectivity at any level; d)

755 maximum 40 dBZ echo top temperature; e) maximum 30 dBZ echo top temperature; f)

756 lightning flash rate. As the percentages of hail PFs in China are much smaller than those

757 in U.S., different vertical coordinates are utilized in each subplot.



758

759 Fig. 8. The median maximum reflectivity profiles of hail Precipitation Features with
 760 different maximum hail diameter (MHD) at high elevation (High) and low elevation
 761 (Low).